MIT Open Access Articles

Efficient Semitransparent CsPbI 3 Quantum Dots Photovoltaics Using a Graphene Electrode

The MIT Faculty has made this article openly available. ***Please share*** how this access benefits you. Your story matters.

Citation	Tavakoli, Mohammad Mahdi, Nasilowski, Michel, Zhao, Jiayuan, Bawendi, Moungi G. and Kong, Jing. 2019. "Efficient Semitransparent CsPbI 3 Quantum Dots Photovoltaics Using a Graphene Electrode." Small Methods, 3 (12).
As Published	http://dx.doi.org/10.1002/smtd.201900449
Publisher	Wiley
Version	Author's final manuscript
Citable link	https://hdl.handle.net/1721.1/140485
Terms of Use	Creative Commons Attribution-Noncommercial-Share Alike
Detailed Terms	http://creativecommons.org/licenses/by-nc-sa/4.0/

Massachusetts Institute of Technology

DSpace@MIT

Check for updates

Efficient Semi-Transparent $CsPbI_3$ Quantum Dots Photovoltaics Using Graphene Electrode

Mohammad Mahdi Tavakoli[1]*, Michel Nasilowski[2], Jiayuan Zhao[1], Moungi G. Bawendi[2], Jing Kong[1]*

[1]*Department of Electrical Engineering and Computer Science, Massachusetts Institute of Technology, Cambridge, MA, USA*

[2]*Department of Chemistry, Massachusetts Institute of Technology, Cambridge, MA, USA*

Corresponding authors:

mtavakol@mit.edu (M.M.T), *jingkong@mit.edu* (J.K.)

Author Manuscript

Abstract

Solution-processed perovskite quantum dots (QDs) are promising candidates for fabrication of semi-transparent and tandem solar cells due to the band gap tunability. In this work, we synthesize $CsPbI_3$ QDs with a stable cubic phase and fabricate efficient perovskite solar cells (PSCs) using the ligand exchange technique. We grow monolayer graphene by chemical vapor deposition (CVD) technique and develop a dry process to transfer graphene on top of the device. Based on this approach, an efficient inverted PSC is demonstrated with a high average visible transmittance (AVT). After optimization, PSCs based on silver and graphene electrodes with power conversion efficiencies (PCEs) of 9.6% and 6.8% are achieved, respectively. Additionally, by tuning the thickness of the active layer, a PSC with PCE of 4.95% and AVT of 53% is demonstrated, indicating the potential of $CsPbI_3$ QDs for the fabrication of semi-transparent devices applicable in windows.

This is the author manuscript accepted for publication and has undergone full peer review but has not been through the copyediting, typesetting, pagination and proofreading process, which may lead to differences between this version and the Version of Record. Please cite this article as doi: 10.1002/smtd.201900449.

This article is protected by copyright. All rights reserved.

Keywords: $CsPbI_3$ QDs, Perovskite, Semi-transparent device, Solar cell, Graphene, Efficiency

Author Manuscript

Introduction

Organic-inorganic perovskite materials with unique crystal structure of ABX_3 (A = organic cation, B = metal, X = halide) have been promising candidates for fabrication of high-performance solar cells due to their alluring advantages such as ease of fabrication, low-cost processing, great light absorption, bandgap tuneability, high carrier mobility and long diffusion length.[1-6] Due to the presence of organic compounds such as methylammonium (MA) in the perovskites, these materials have stability issue, especially in a humid environment, hindering their practical applications.[7-11] Fabrication of all inorganic perovskite films such as cesium lead triiodide ($CsPbI_3$) is an effective way to address this issue. Interestingly, it was found that $CsPbI_3$ perovskite with a black cubic phase has a band gap of 1.72 eV, which is suitable for optoelectronic devices.[12-15] However, this material has a poor phase stability, *i.e.*, the cubic phase of $CsPbI_3$ perovskite is converted to a yellow orthorhombic phase at temperatures below 310 °C, which has much lower light absorption.[16-18] Therefore, stabilization of the cubic phase at room temperature has been a bottleneck challenge in the fabrication of stable $CsPbI_3$ perovskite solar cells (PSCs). To overcome this issue, two strategies have been developed, compositional engineering[19] and phase confinement.[20] In this regard, most people have worked on the composition of perovskite films by adding halide salts, organic compounds, and metal elements to increase the entropy and thus the stability of the system.[22,23] For instance, Lau et al.[24] tuned the composition of $CsPbI_3$ perovskite films by incorporation of calcium and stabilized the cubic phase of the perovskite film, resulting in a PSC device with over 13% efficiency. In the case of phase confinement, previously, Waleed et. al.[20] successfully grew stable $CsPbI_3$ nanowire

This article is protected by copyright. All rights reserved.

perovskite with cubic phase inside anodized aluminum oxide membranes using CVD technique for photo-detecting application. Swarnkar et al.[25] synthesized $CsPbI_3$ QDs perovskite using hot injection method and improved the mobility of the perovskite film using organic salts such as formamidinium iodide (FAI). Using this approach, they showed a $CsPbI_3$ QDs PSC with a certified efficiency of 13.2%.

In fact, $CsPbI_3$ QDs could be a potential candidate for the fabrication of semi-transparent solar cells. Compared to the bulk perovskite materials, $CsPbI_3$ QDs can be processed in ambient air and at room temperature with good stability and without damage. Also, the thickness of the active layer can be easily tuned through layer-by-layer film deposition with a better uniformity, smoothness and film coverage than a bulk thin film.[26] In order to make a semi-transparent device, it is necessary to find an alternative top electrode with high transmittance. Since a monolayer of graphene has a good conductivity with a high transmittance of 98%, it is an excellent candidate for this purpose.[27-29] However, an effective way to transfer the graphene on top of the perovskite film, without deterioration of the device performance, is required. Due to the above advantages of $CsPbI_3$ QDs films, especially air-stability, graphene is an interesting choice for the fabrication of a semi-transparent $CsPbI_3$ QDs PSC. In fact, there are other alternative electrodes for the fabrication of semi-transparent PSCs such as indium-doped tin oxide (ITO)[30] and thin metal[31], however, they required an additional step using vacuum deposition, which increases the price as compared to the graphene electrode. Up to now, most of the semi-transparent PSCs reported in the literature has very low AVT below 35%,[32] which is not suitable for application in window. Consequently, combining graphene with $CsPbI_3$ QDs solar cell could be a good solution to not only reduce the price but also increase the AVT of the device.

Author Manuscript

This article is protected by copyright. All rights reserved.

In this work, we successfully transfer CVD graphene on top of $CsPbI_3$ QDs perovskite films as a transparent electrode using a dry process. We fabricate an inverted PSC device using $CsPbI_3$ QDs and replace the silver electrode with graphene on top of the device using ethylene-vinyl-acetate (EVA) as an adhesive material and polydimethylsiloxane (PDMS) as a stamp. Based on this approach, we demonstrate a semi-transparent device with a PCE of 4.95% as well as an AVT of 53% over the visible spectrum. These values are among the best reported values in the literature for the semi-transparent PSCs.[28]

Results and discussion

We synthesize $CsPbI_3$ QDs using a hot injection method as explained in the experimental section and characterize them as shown in Figure 1. High resolution transmission electron microscopy (HRTEM) results show that the QDs have a cubic shape with uniform size distribution. The average size of the dots is around 9 nm (Figure 1a). The inset image in Figure 1a indicates an interplanar distance of 0.62 nm, which corresponds to the (100) planes of the cubic phase of the $CsPbI_3$.[25] Figure 1b shows the optical characterization of $CsPbI_3$ QDs in the solution phase. From the UV-visible spectrum, the bandgap is around 1.81 eV and the QDs show a strong photoluminescence (PL) peak (The inset image shows the strong emission of the dots under UV light) with PL quantum yield (PLQY) of 70%.

To fabricate $CsPbI_3$ QDs films, a ligand exchange technique is employed as reported in the literature.[26] We exchange the long oleic acid ligands with lead nitrate and, in order to improve the mobility of the perovskite film, the surface of $CsPbI_3$ QDs films is treated with FAI.[26] Figure 1c shows the optical characterization of the resulting $CsPbI_3$ QDs film. As seen in Figure 1c, the film shows a slight red-shifted PL peak as compared to the QDs in the solution phase (Figure 1b). This is due to a shorter interparticle distance and an increase in

This article is protected by copyright. All rights reserved.

Author Manuscript

QD-QD energy transfer. The band gap of the film is estimated from both UV-visible and PL spectra to be ~1.79 eV. Figure 1d shows an atomic force microscopy (AFM) image of a $CsPbI_3$ QDs film. The AFM imaging indicates a smooth film with a roughness of 4.5±1.5 nm (see Figure S1). Moreover, the crystal structure of the $CsPbI_3$ QDs film is investigated using two-dimensional X-ray diffraction (2D-XRD), as shown in Figure S2. This result confirms the cubic structure of $CsPbI_3$ film after ligand exchange.[24]

Since $CsPbI_3$ QDs perovskites are stable in ambient air due to the lack of organic compounds, the top graphene-based device is fabricated under ambient condition without using a nitrogen-filled glovebox. To transfer graphene on top of the device, we employ a dry process[27] for the $CsPbI_3$ QDs PSC, as schematically shown in Figures 2a-2d. We could not use wet transfer technique in this work (see Figure S3), due to the presence of lead nitrate ligands on the surface of $CsPbI_3$ QDs after deposition, which are soluble in water. The details of this transfer process can be found in the experimental section. Briefly, a monolayer of graphene is synthesized using chemical vapor deposition (CVD) on the surface of copper foil. Then, thin layers of EVA and poly(methyl methacrylate) (PMMA) are deposited on top of graphene/copper as an adhesive and a protective layer, respectively. Here, we use two layers of graphene to decrease the sheet resistance of the final electrode below 200 ohm/sq.[27] For the dry transfer process, a PDMS stamp with a hole in its center is employed to facilitate detaching graphene from the stamp. As shown in Figure 2a, the PDMS stamp is pressed on top of the PMMA/EVA/graphene/copper stack and then the copper foil is etched away from the stack in a copper etchant solution (Figure 2b). Afterwards, the graphene membrane together with PDMS is stamped on top of the PSC device gently and heated up to 70 $^{\circ}$C for 5 min, as schematically shown in Figure 2c. During the heating step, the PDMS is removed slowly from the graphene membrane, resulting in a device with a top graphene electrode (Figure 2d). Figures 2e and 2f show the schematic and cross-sectional-view SEM image of an

This article is protected by copyright. All rights reserved.

inverted PSC device based on $CsPbI_3$ perovskite QDs. As seen, the device consists of an ITO glass, a 10 nm-thick layer of Poly[bis(4-phenyl)(2,4,6-trimethylphenyl)amine] (PTAA) as a hole transporting layer (HTL), a $CsPbI_3$ QDs film as an absorber layer, a 23 nm-thick layer of C60 as an electron transporting layer (ETL), a 8 nm-thick bathocuproine (BCP) film as a buffer layer and Ag (100 nm) or graphene as back contact electrodes. $CsPbI_3$ QDs films are fabricated using the procedure reported by Sanehira et al.[26] Figure S4 shows ultraviolet photoelectron spectroscopy (UPS) of $CsPbI_3$ QDs films and graphene layer with their corresponding band diagram. From the UPS and UV-visible results, the valence band (VB) and conduction band (CB) of $CsPbI_3$ films are estimated to be 5.69 eV and 3.9 eV, respectively. These values are well-matched with the VB of PTAA and the CB of C60, as shown in Figure S4. Additionally, based on UPS result, the work function of the graphene electrode is estimated to be 4.67 eV, which is suitable to replace Ag electrode in the inverted PSC architecture.

To study the role of graphene as a top electrode, PSCs with both Ag and graphene electrodes are fabricated and characterized. Figure 3 shows the photovoltaic (PV) results of the PSCs with Ag and graphene electrodes measured under standard AM1.5G conditions. The current density-voltage (*J-V*) curves and the figures of merit for the corresponding PSCs are shown in Figure 3a and Table 1, respectively. The device, based on a silver electrode, demonstrates a typical PCE of 9.6% with a J_{sc} of 11.8 mA/cm^2, a V_{oc} of 1108 mV, and a fill factor (FF) of 73.5% under reverse scan, while the device based on graphene electrode yields a lower PCE of 6.8% with a V_{oc} of 1090 mV, a J_{sc} of 10.9 mA/cm^2, and a lower FF of 57.5% under reverse scan. This may be attributed to the higher sheet resistance of the graphene electrode and the contact of graphene electrode with the underneath layers. The sheet resistance of graphene is about 200 ohm/sq, which is much higher than that of Ag electrode. Moreover, during the transfer process, there is some possibility of having trapped air at the

This article is protected by copyright. All rights reserved.

Author Manuscript

interface of graphene with the underneath layers and thus these issues can potentially affect on the FF and PCE of the graphene-based device as compared to the reference device. For the current density, an opaque device with metal electrode shows higher J_{sc} than a semi-transparent device, due to the reflectance effect of the metal electrode.[27] To improve the FF of the graphene-based PSCs, we employed two layers of graphene on top the device. Table S1 shows the effect of number of graphene layers on the device parameters. As seen, by adding more graphene layers, the FF and thus PCE are increased slightly, due to better conductivity of top electrode. However, by adding more graphene layers, the AVT of the device is dropped. In this study, we find that usage of two graphene layers is the optimum condition for obtaining high PCE as well as high AVT. Additionally, we study the effect of active areas in the photovoltaic parameters of the PSCs, as summarized in Table S2. Our results show that by increase the active area (defined by shadow mask), the FF, J_{sc}, and thus PCE are dropped slightly, which is mainly due to higher sheet resistance of larger graphene electrode. As seen in Figure 3a, our devices also depict negligible hysteresis. Figure 3b shows the maximum power point tracking (MPPT) of the corresponding PSCs. The MPP for the devices with Ag and graphene electrodes are 9.2% and 6.4%, respectively, indicating their stability over one minute under illumination with a low hysteresis effect. Figure S5 shows the average values of the hysteresis indices of the PSCs ($HI=[(PCE_{backward}-PCE_{forward})/PCE_{backward}]*100$), which are below 2%. We find that the PSCs with graphene electrodes have smaller HI as compared to PSCs with Ag electrode. To confirm the current density of the PSCs, we measure the external quantum efficiency (EQE) of the corresponding devices and extract the J_{sc} from the EQE results, as shown in Figure 3c. The calculated J_{sc} from the EQE results is 10.4 and 9.5 mA/cm^2 for devices with Ag and graphene electrodes, respectively, which are in good agreement with the *J-V* results (Figure 3a).

Author Manuscript

This article is protected by copyright. All rights reserved.

Figures 3d and S6 demonstrate the statistics of the PV parameters for the PSCs with Ag and graphene electrodes (10 devices for each electrode). As seen, the average values of J_{sc}, FF, and PCE for the device with graphene electrode are lower than those of the device with Ag electrode, due to a lower conductivity of graphene as compared to Ag electrode.

Table 1. Figures of merit for the champion PSCs with Ag and graphene electrodes under reverse and forward scan directions

Device	V_{oc} (mV)	J_{sc} (mA/cm^2)	FF (%)	PCE (%)	J_{sc} from EQE (mA/cm^2)
Ag-backward	**1108**	**11.8**	**73.5**	**9.6**	**10.4**
Ag-forward	**1097**	**11.62**	**73.9**	**9.42**	
Graphene-backward	**1090**	**10.9**	**57.5**	**6.8**	**9.5**
Graphene-forward	**1081**	**10.79**	**57.7**	**6.73**	

To study the transmittance of the PSCs, we tune the thickness of the $CsPbI_3$ absorber layer through deposition from 1 to 3 layers. The J-V results of the corresponding PSCs are listed in Table 2. As seen, by reducing the thickness of the absorber layer from 3 layers to 1 layer, the PCE is dropped from 5.9% to 3.2%, while the AVT is increased from 39% to 68%. Our results show that the device with 2 layers of $CsPbI_3$ QDs has a reasonable PCE of 4.95% with a high AVT of 53%, indicating a proper balance between transmittance and PCE. Figure 4a shows the transmittance spectrum of the $CsPbI_3$ QDs PSC with graphene top electrode. The inset image and Figure 4b depict the photographs of the corresponding device, indicating its high transmittance. The J-V curves of the corresponding PSC with graphene electrodes are measured from both top and bottom sides of the device (Figure 4c). When the device is measured from the graphene side, the current density is slightly increased from 8.01 to 8.30 mA/cm^2, resulting in a PCE enhancement from 4.95% to 5.11%. This indicates that the graphene electrode has better transmittance than ITO through the entire solar spectrum,

This article is protected by copyright. All rights reserved.

Author Manuscript

especially in the UV regions. In order to further study this point, we measured the EQE spectra of the PSCs from ITO and graphene sides as shown in Figure 4d. As seen, by measuring from the graphene side, the EQE values are higher than its counterpart, especially in the UV region, indicating the better transmittance of graphene electrode.

As mentioned in the literature, stability is the main challenge in the field of PSCs.[33-37] Therefore, we measured the shelf-life stability of our devices in ambient air (20% RH) over 14 days. Figures 5a and 5b show the contact angle (CA) of water droplet on top of the PSCs with Ag and graphene electrodes, respectively. As seen, the CAs are 52° for Ag and 109° for graphene electrodes, indicating that graphene electrode can protect the PSC in humid environment as compared to the Ag one. Figure 5c shows the shelf-life stability of the corresponding devices, kept in a dark condition with 20% RH over time. Our result reveals that the graphene-based PSC retains more than 96% of its initial PCE value after 14 days, indicating its great air stability as compared to the Ag-based PSC. The PSC with Ag electrode maintains 91% of its initial PCE value after 14 days, demonstrating its lower stability, mainly due to the oxidation of silver electrode in the air.

Table 2. Figures of merit for the PSC devices with graphene electrode and different thicknesses of the $CsPbI_3$ QDs layer under reverse scan direction

Number of $CsPbI_3$ layer	V_{oc} (mV)	J_{sc} (mA/cm^2)	FF (%)	PCE (%)	AVT (%) (Thickness of $CsPbI_3$ (nm))
1	**1092±11**	**5.2±0.82**	**56.4±3.4**	**3.2±0.7**	**68** (103)
2	**1091±12**	**8.3±0.92**	**57.1±4.3**	**4.9±0.8**	**53** (192)
3	**1087±13**	**10.4±0.85**	**54.2±4.8**	**5.9±0.9**	**39** (293)

In order to compare the PCE and AVT of our semi-transparent device with the state of art in the literature, we plotted a PCE versus AVT graph containing our best performing

This article is protected by copyright. All rights reserved.

Author Manuscript

device and the best performing semi-transparent PSCs reported in the literature.[32] As shown in Figure S7, most of the reported PSCs have PCE in range of 7-12% and low AVT of 20-35%. In contrast, our device shows a decent PCE of 4.95% and a very high AVT of 53%. These results indicate that our semi-transparent device could be a better choice for application in the windows as compared to the devices reported in the literature due to its higher transmittance.

Conclusions

In summary, we synthesize stable cubic phase of $CsPbI_3$ QDs and fabricate PSC devices using ligand exchange under ambient conditions. We find that $CsPbI_3$ perovskite QDs are good candidates for the fabrication of semi-transparent PV devices. We employ CVD graphene as a top electrode and develop a dry transfer process for graphene. After optimization, we achieve inverted PSC devices with efficiencies of 9.6% and 6.8% based on Ag and graphene electrodes, respectively. Moreover, we show a semi-transparent $CsPbI_3$ QDs PSC with a PCE of 4.95% and an AVT of 53%, indicating that $CsPbI_3$ QDs is a suitable candidate for window applications.

Experimental section

Growth of graphene: Low-pressure chemical vapor (LPCVD) deposition was used to grow monolayer graphene on copper foil (Alfa Aesar). After cleaning the copper foil in a nickel etchant bath (Transene, type TFB) by sonification for 2 min and rinsing, the graphene has been grown on copper foil in a CVD furnace as reported elsewhere.[5,25]

Transfer process of graphene: For graphene transfer, a dry transfer process was used. A 40 nm-thick EVA layer was spin-coated on the copper foil, followed by spinning a 300 nm-thick of PMMA at 4000 rpm for 60s. Then, the copper/graphene/EVA/PMMA stack was annealed at 75 °C for 3h. In order to perform a dry transfer process, a PDMS mold with a hole in its

This article is protected by copyright. All rights reserved.

Author Manuscript

center was attached to the PMMA side to handle the stack easily. Then, the copper foil was etched away from the stack by floating it on a $FeCl_3$-based copper etchant (Transene). Afterward, the graphene/EVA/PMMA/PDMS stack was washed in deionized (DI) water bath several times and then in a diluted HCL bath (10%vol). After washing the stack in DI water bath and drying, the stack was stamped on top of the device to transfer the graphene as a top electrode. Finally, the PDMS was removed from the stack by heating the device at 70 °C for 5 min.

Synthesis of $CsPbI_3$ QDs: $CsPbI_3$ QDs were synthesized according to the procedure reported in the literature.[24] Briefly, 0.407 g of Cs_2CO_3, 1.25 ml of oleic acid (OA), and 20 ml of octadecene (ODE) were mixed and degassed in a three-neck flask under vacuum at 120 °C for 30 min to obtain Cs oleate in ODE solution with concentration of 0.125 M. Then, nitrogen was purged into the flux and the temperature was set to 150 °C, yielded a clear solution. Afterward, 0.5 g of PbI_2 and 25 mL of ODE were stirred and dissolved in a separated flask at 120°C for 30 min, followed by adding 2.5 mL from each preheated (130 °C) OA and oleylamine (OAm) to the flask. To synthesize $CsPbI_3$ QDs, the temperature of the flask was increased to 180 °C, while purging nitrogen and then 2 mL of the preheated Cs-oleate (130 °C, 0.125 M) was injected into the flask. After 10 s, the flask was quenched in an ice bath. To isolate the QDs, 35 mL of methylacetate (MeOAc) was added to 15 mL QDs solution, followed by centrifuging at 7500 rpm for 5 min. Afterward, the supernatant was removed, and the dots were redispersed in a sufficient amount of hexane. The dots were purified several times using MeOAc and finally dispersed in hexane and stored in the dark at 4 °C.

Device fabrication: The patterned ITO glass was cleaned in the following bathes, 3vol% triton X100 in DI water, DI water, Acetone, ethanol. After drying, the surface of ITO glass was cleaned by oxygen plasma for 2 min. Then, an 8 nm-thick of poly(triarylamine) (PTAA, Sigma-Aldrich) was deposited from a solution of 2 mg/mL toluene at 6000 rpm for 40 s (with

This article is protected by copyright. All rights reserved.

Author Manuscript

acceleration rate of 2000 rpm/s). The PTAA film was annealed at 100 °C for 10 min in a nitrogen glovebox.

$CsPbI_3$ QDs film was deposited by spin coating of a QDs solution of 80 mg/mL in octane at 1000 rpm for 30 s, followed by 2000 rpm for 5 s. To obtain enough thickness for the $CsPbI_3$ QDs, the process was repeated three times. (Notable, the efficiency is dropped upon adding the forth layer). Between each deposition step, the films were dipped into a saturated solution of $Pb(NO_3)_2$ in MeOAc and pure MeOAc for 1 s, respectively. After finishing the deposition and drying the layer, the film was further dipped into the saturated solution of FAI in ethylacetate (EtOAc) to improve the mobility of the $CsPbI_3$ QDs perovskite. The fabrication process of QDs film was performed in the air with 20% relative humidity (RH). After deposition of $CsPbI_3$ QDs layer, the samples were transferred into a thermal evaporator and C60 (23 nm), BCP (8 nm), and silver (100 nm) were thermally evaporated on top of the film under vacuum of 10^{-7} mbar to complete the device fabrication.

Film characterization: $CsPbI_3$ film was characterized by a high-resolution scanning electron microscopy (HRSEM, ZEISS Merlin), Atomic force microscopy (AFM, NanoScope IIIa/Dimension 3100) and x-ray diffraction (XRD, Bruker D8 X-ray Diffractometer (USA) with GADDS utilizing a Co radiation). A Varian Cary 5 and a Fluorolog 322 (Horiba Jobin Ybon Ltd) were employed to measure the UV–visible and photoluminescence (PL) spectra, respectively. The band diagram of the $CsPbI_3$ QDs was analyzed by ultraviolet photoelectron spectroscopy (UPS) in an Omicron ultrahigh vacuum system using a He I line (21.2 eV) of a helium discharge lamp.

Device characterization: All devices were measured using a digital source meter (Keithley model 2400, USA) and a 450 W xenon lamp (Oriel, USA). A Schott K113 Tempax sunlight filter (Präzisions Glas & Optik GmbH, Germany) and standard silicon solar cell (Newport)

Author Manuscript

This article is protected by copyright. All rights reserved.

was used to match the emission spectra of the lamp to the AM1.5G standard. The device area was 0.054 cm^2, which was defined by shadow mask. The voltage scan rate and the dwell time were set to 50 mV/s and 15 s, respectively. The light intensity was 1000 W/m^2 in accordance with standard AM 1.5G. For external quantum efficiency (EQE) measurement, a commercial apparatus (Arkeo-Ariadne, Cicci Research s.r.l.) with a 300 Watts Xenon lamp was used.

Acknowledgement

This work was sponsored by ENI S.p.A under the MITEI Solar Frontier Center.

References

1. N. G. Park, M. Grätzel, T. Miyasaka, K. Zhu, K. Emery, *Nat. Energy* **2016**, *1*, 16152.

2. M. M. Tavakoli, S.M. Zakeeruddin, M. Grätzel, Z. Fan, *Adv. Mater.* **2018,** *30*, 1705998.

3. J. W. Lee, H. S. Kim, N. G. Park, *Acc. Chem. Res.* **2016**, *49,* 311-319.

4. N. J. Jeon, H. Na, E. H. Jung, T. Y. Yang, Y. G. Lee, G. Kim, H. W. Shin, S. I. Seok, J. Lee, J. Seo, *Nat. Energy* **2018,** *3*, 682.

5. National Center for Photovoltaics (NCPV) at the National Renewable Energy Laboratory (NREL) efficiency chart www.nrel.gov/pv/assets/images/efficiency-chart.png.

6. M. M. Tavakoli, W. Tress, J. V. Milić, D. Kubicki, L. Emsley, M. Grätzel, *Energy Environ. Sci.* **2018,** *11,* 3310.

7. N. J. Jeon, J. H. Noh, W. S. Yang, Y. C. Kim, S. Ryu, J. Seo, S. I. Seok, *Nature* **2015**, *517,* 476.

8. M. M. Tavakoli, R. Tavakoli, P. Yadav, J. Kong, *J. Mater. Chem. A* **2019**, *7,* 679-686.

9. D. Prochowicz, M. M. Tavakoli, A. Solanki, T. W. Goh, K. Pandey, T. C. Sum, M. Saliba, P. Yadav, *J. Mater. Chem. A* **2018**, *6*, 14307-14314.

10. M. M. Tavakoli, P. Yadav, D. Prochowicz, M. Sponseller, A. Osherov, V. Bulović, J. Kong, *Adv. Energy Mater.* **2019**, 1803587.

This article is protected by copyright. All rights reserved.

Author Manuscript

11. D. Prochowicz, P. Yadav, M. Saliba, D. J. Kubicki, M. M. Tavakoli, S. M. Zakeeruddin, J. Lewiński, L. Emsley, M. Grätzel, *Nano Energy*, **2018**, *49*, 523-528.

12. G. E. Eperon, G. M. Paterno, R. J. Sutton, A. Zampetti, A. A. Haghighirad, F. Cacialli, H. J. Snaith, *J. Mater. Chem. A* **2015**, *3*, 19688-19695.

13. J. Liang, P. Zhao, C. Wang, Y. Wang, Y. Hu, G. Zhu, L. Ma, J. Liu, Z. Jin, *JACS* **2017**, *139,* 14009-14012.

14. Y. Hu, F. Bai, X. Liu, Q. Ji, X. Miao, T. Qiu, S. Zhang, *ACS Energy Lett.* **2017**, *2*, 2219-2227.

15. X. Li, M. I. Dar, C. Yi, J. Luo, M. Tschumi, S. M. Zakeeruddin, M. K. Nazeeruddin, H. Han, M. Grätzel, *Nat. Chem.* **2015**, *7,* 703.

16. Q. Ma, S. Huang, X. Wen, M. A. Green, A. W. Ho-Baillie, *Adv. Energy Mater.* **2016**, *6,* 1502202.

17. R. E. Beal, D. J. Slotcavage, T. Leijtens, A. R. Bowring, R. A. Belisle, W. H. Nguyen, G. F. Burkhard, E. T. Hoke, M. D. McGehee, *J. Phys. Chem. Lett.* **2016**, *7,* 746-751.

18. T. Zhang, M. I. Dar, G. Li, F. Xu, N. Guo, M. Grätzel, Y. Zhao, *Sci. Adv.* **2017**, *3*, e1700841.

19. C. Y. Chen, H. Y. Lin, K. M. Chiang, W. L. Tsai, Y. C. Huang, C. S. Tsao, H. W. Lin, *Adv. Mater.* **2017**, *29*, 1605290.

20. A. Waleed, M. M. Tavakoli, L. Gu, S. Hussain, D. Zhang, S. Poddar, Z. Wang, R. Zhang, Z. Fan, *Nano Lett.* **2017**, *17*, 4951-4957.

21. L. A. Frolova, D. V. Anokhin, A. A. Piryazev, S. Y. Luchkin, N. N. Dremova, K. J. Stevenson, P. A. Troshin, *J. Phys. Chem. Lett.* **2016**, *8,* 67-72.

22. J. K. Nam, S. U. Chai, W. Cha, Y. J. Choi, W. Kim, M. S. Jung, J. Kwon, D. Kim, J. H. Park, *Nano Lett.* **2017**, *17,* 2028-2033.

23. M. Kulbak, D. Cahen, G. Hodes, *J. Phys. Chem. Lett.* **2015**, *6*, 2452-2456.

This article is protected by copyright. All rights reserved.

24. C. F. J. Lau, X. Deng, J. Zheng, J. Kim, Z. Zhang, M. Zhang, J. Bing, B. Wilkinson, L. Hu, R. Patterson, S. Huang, *J. Mater. Chem. A* **2018***, 6,* 5580-5586.

25. A. Swarnkar, A. R. Marshall, E. M. Sanehira, B. D. Chernomordik, D. T. Moore, J. A. Christians, T. Chakrabarti, J. M. Luther, *Science* **2016**, *354*, 92-95.

26. E. M. Sanehira, A. R. Marshall, J. A. Christians, S. P. Harvey, P. N. Ciesielski, L. Wheeler, P. Schulz, L. Y. Lin, M. C. Beard, J. M. Luther, *Sci. Adv.* **2017**, *3*, p.eaao4204.

27. Y. Song, S. Chang, S. Gradecak, J. Kong, *Adv. Energy Mater.* **2016***, 6*, 1600847.

28. L. Yuan, Z. Wang, R. Duan, P. Huang, K. Zhang, Q. Chen, N. K. Allam, Y. Zhou, B. Song, Y. Li, *J. Mater. Chem. A* **2018**, *6,* 19696-19702.

29. P. You, Z. Liu, Q. Tai, S. Liu, F. Yan, *Adv. Mater.* **2015***, 27,* 3632-3638.

30. K. A. Bush, C. D. Bailie, Y. Chen, A. R. Bowring, W. Wang, W. Ma, T. Leijtens, F. Moghadam, M. D. McGehee, *Adv. Mater.* **2015***, 28,* 3937-3943.

31. S. P. Cho, S. I. Na, S. S. Kim, *Sol. Energy Mater. Sol. Cells* **2019**, *196*, 1-8.

32. Q. Xue, R. Xia, C. J. Brabec, H. L. Yip, *Energy Environ. Sci.* **2018***, 11,* 1688-1709.

33. M. M. Tavakoli, P. Yadav, D. Prochowicz, M. Sponseller, A. Osherov, V. Bulović, J. Kong, *Adv. Energy Mater.* **2019**, *9*, 1803587.

34. M. M. Tavakoli, M. Saliba, P. Yadav, P. Holzhey, A. Hagfeldt, S. M. Zakeeruddin, M. Grätzel, *Adv. Energy Mater.* **2019***, 9,* 1802646.

35. M. M. Tavakoli, D. Bi, L. Pan, A. Hagfeldt, S. M. Zakeeruddin, M. Grätzel, *Adv. Energy Mater.* **2018***, 8,* 1800275.

36. A. Tayyebi, M. M. Tavakoli, M. Outokesh, A. Shafiekhani, A. Simchi, *Ind. Eng. Chem. Res.* **2015**, *54,* 7382-7392.

37. M. Yavari, M. Mazloum-Ardakani, S. Gholipour, M. M. Tavakoli, S. H. Turren-Cruz, N. Taghavinia, M. Grätzel, A. Hagfeldt, M. Saliba, *Adv. Energy Mater.* **2018***, 8*, 1800177.

This article is protected by copyright. All rights reserved.

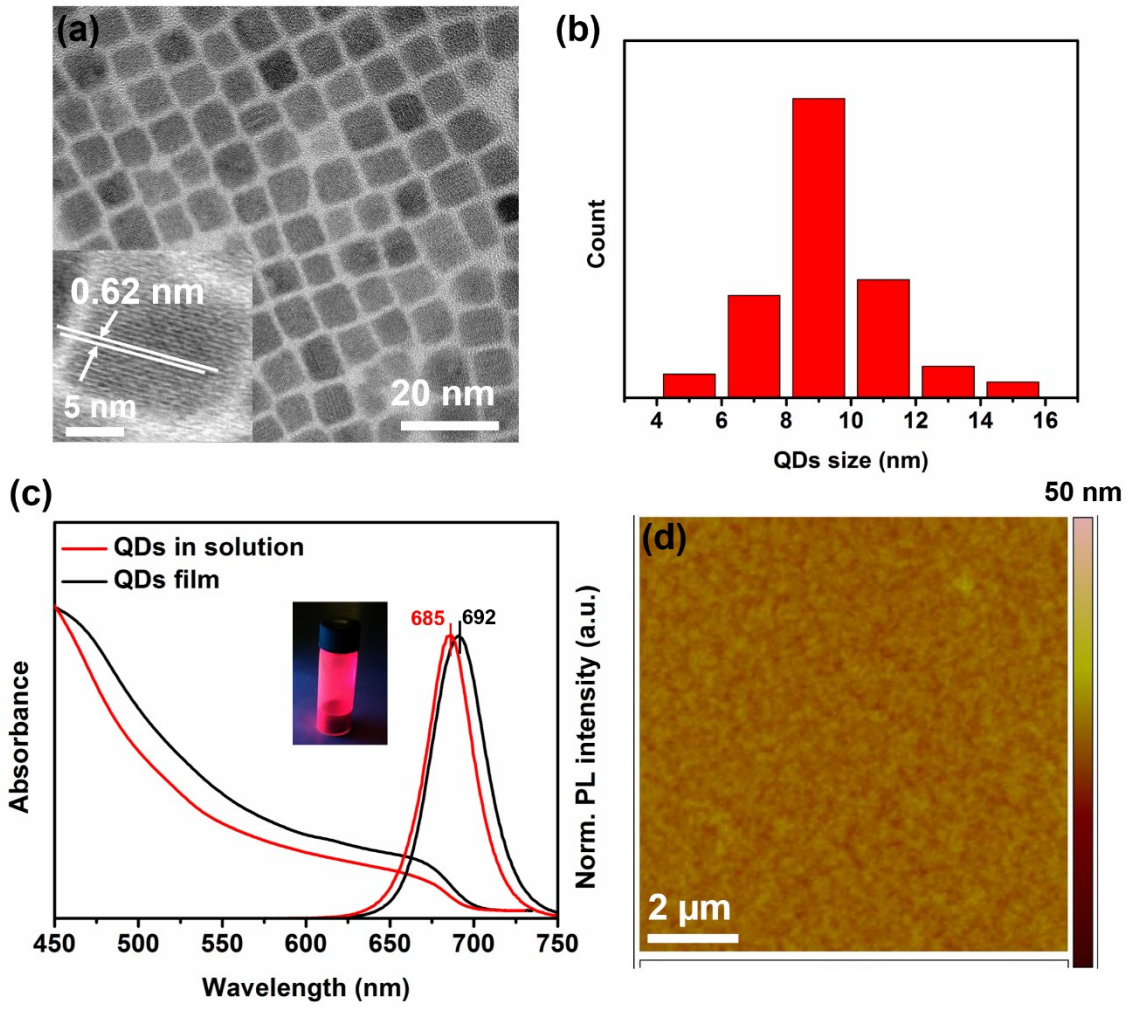

Figure 1. (a) HRTEM image of $CsPbI_3$ QDs with a uniform size distribution. The inset image shows the fringes of one cubic dot with higher magnification. (b) Histogram of particle size distribution for $CsPbI_3$ QDs estimated from TEM images. (c) UV-visible absorption and photoluminescence spectra of $CsPbI_3$ QDs dispersed in the solution and $CsPbI_3$ QDs thin film deposited on glass. The inset image shows the emission of these dots under UV light. (d) AFM image of the corresponding QDs film.

This article is protected by copyright. All rights reserved.

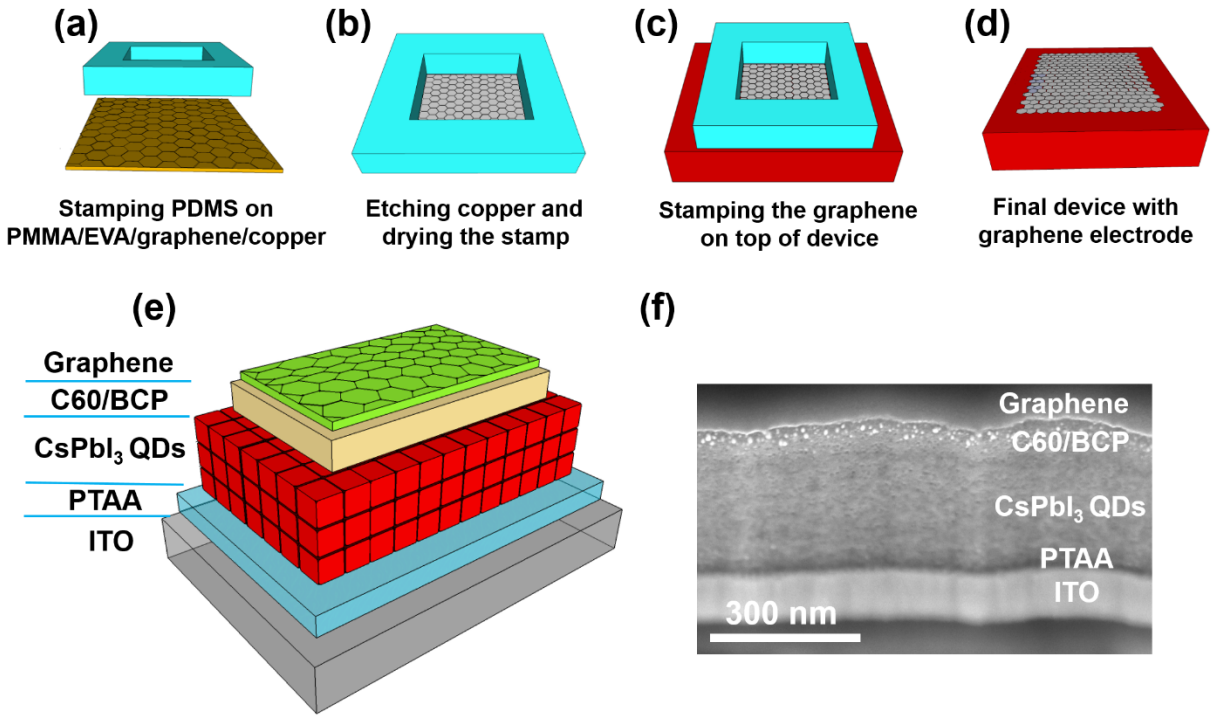

Figure 2. Dry-transfer process of graphene on top of PSC device, (a) Stamping PDMS mold on top of graphene/copper coated by EVA and PMMA respectively, (b) Etching copper and drying the remaining part with graphene gently, (c) Stamping the graphene with its polymer protection, and (d) Heating the device up to 75 °C and gently removing the PDMS stamp. (e) Schematic of an inverted PSC device based on $CsPbI_3$ QDs as an absorber layer. (f) Cross-section SEM image of the corresponding device architecture.

Author Manuscript

This article is protected by copyright. All rights reserved.

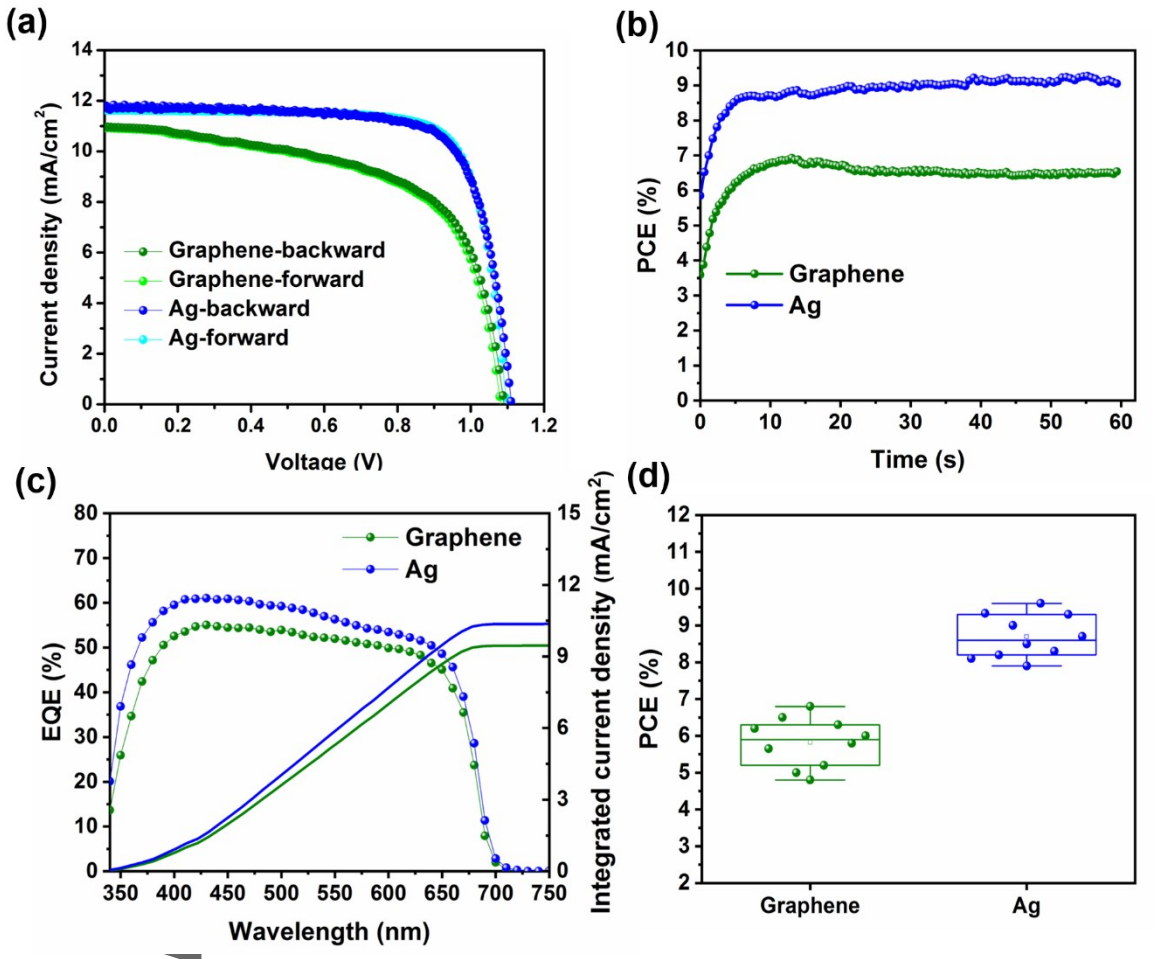

Figure 3. (a) *J-V* curves with forward and reverse scans, (b) MPPT curves, (c) EQE spectra of champion PSC devices with graphene and Ag electrodes. (d) Statistic of PCE for the corresponding PSCs.

Author M

This article is protected by copyright. All rights reserved.

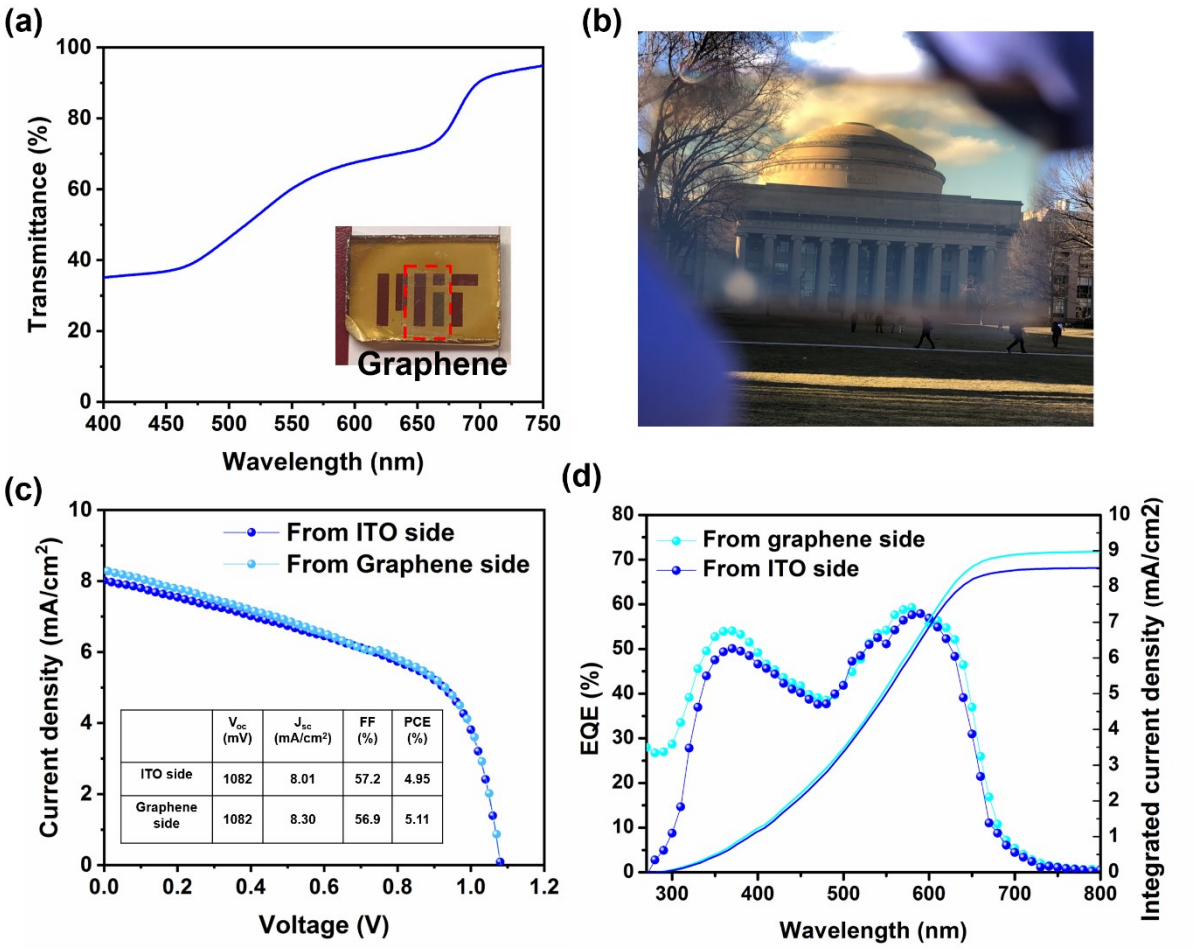

	V_{oc} (mV)	J_{sc} (mA/cm²)	FF (%)	PCE (%)
ITO side	1082	8.01	57.2	4.95
Graphene side	1082	8.30	56.9	5.11

Figure 4. (a) Transmittance spectrum of $CsPbI_3$ PSC device with graphene electrode. Inset image is the photograph of the corresponding device. (b) Photograph of the semi-transparent $CsPbI_3$ PSC. (c) J-V curves and (d) EQE spectra of the semi-transparent $CsPbI_3$ PSC measured from graphene and ITO sides. Inset table shows the figures of merit for this device measured from the both sides.

Author N

This article is protected by copyright. All rights reserved.

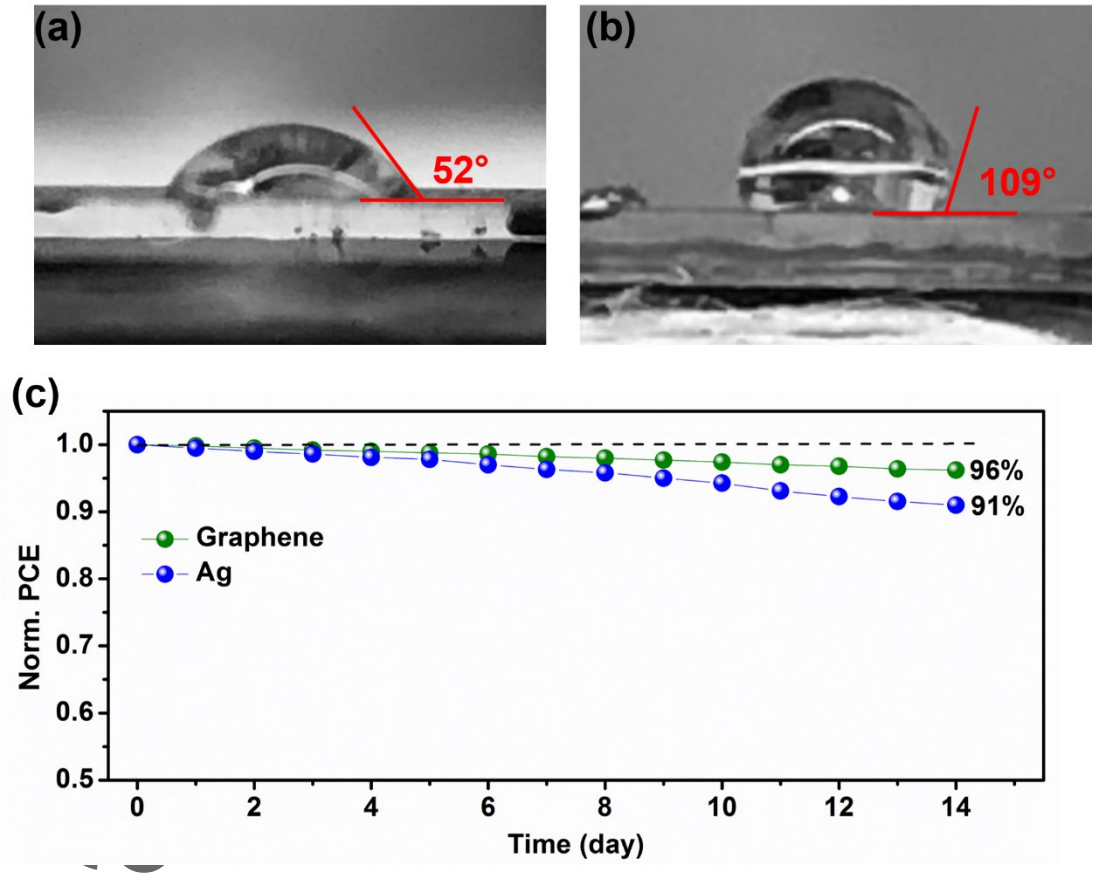

Figure 5. Contact angle measurement of water droplet on top of the PSCs with Ag (a) and graphene (b) electrodes. (c) Shelf-life stability test for the corresponding PSCs in ambient air (20% RH).

Author M

This article is protected by copyright. All rights reserved.

TOC

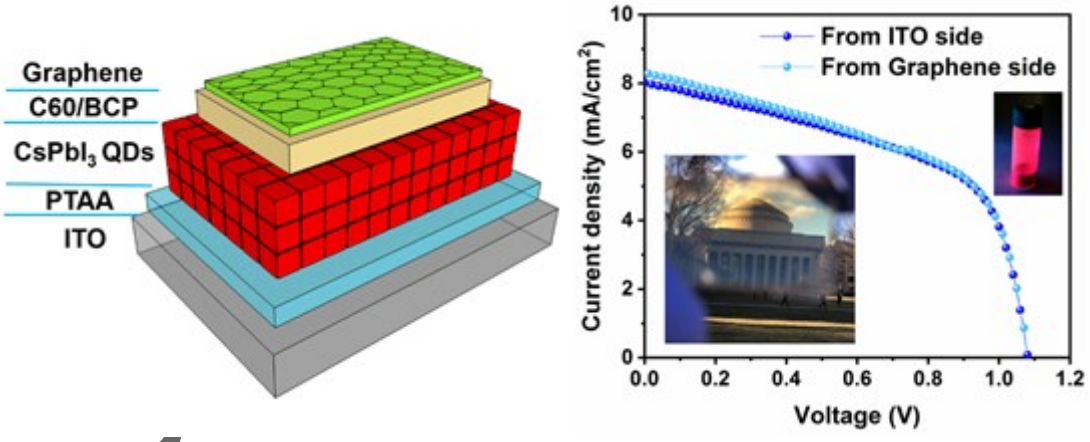

Combination of $CsPbI_3$ QDs absorber layer with graphene electrode in an inverted perovskite solar cell is a great strategy for the fabrication of semi-transparent device with PCE of 4.95% and high AVT of 53%, which is applicable in windows.

Author Manuscript

This article is protected by copyright. All rights reserved.